THE ASTROPHYSICAL JOURNAL, Vol. 157, July 1969

THE HARD SOLAR X-RAY SPECTRUM OBSERVED FROM THE THIRD ORBITING SOLAR OBSERVATORY

HUGH S. HUDSON, LAURENCE E. PETERSON,
AND DANIEL A. SCHWARTZ
University of California, San Diego
Received December 9, 1968; revised January 23, 1969

ABSTRACT

The hard solar X-ray scintillation-counter telescope on the OSO-III satellite covers the energy range 7.7–210 keV with 15-sec time resolution, and six logarithmically spaced energy channels. Approximately 55 per cent time coverage has been obtained for the period following the date of launching, March 8, 1967, until failure of the on-board tape recorder June 28, 1968 This paper is based mainly on solar X-ray events observed during the first two weeks of data accumulation. Approximately ten bursts per day were detected during the interval March 9–March 23, 1967, above the threshold sensitivity of 10^{-8} erg $(\text{cm}^2\ \text{sec})^{-1}$ for $7.7 \leq h\nu \leq 12.5$ keV. About once per day a burst of peak energy flux greater than 1.6×10^{-5} erg $(\text{cm}^2\ \text{sec})^{-1}$ was observed. Although many variations were observed, the typical event had an e-folding rise time of 86 sec and a decay time of 458 sec. The bursts occurred in correlation with almost all listed flares and subflares (88 per cent), microwave bursts (92 per cent), and SID's (100 per cent). Numerous bursts were also detected without these accompanying phenomena. The correlation with type III radio bursts, although still positive, is not as good (31 per cent), a fact which suggests that coronal disturbances are not an inevitable consequence of the process which produces X-ray emission. The X-ray spectrum is appreciably non-thermal in the initial phase of the burst and thermal in the decay phase, with an effective temperature often exceeding 50×10^6 ° K. The average peak temperature of subflares exceeds 10×10^6 ° K, while that of importance 1 or greater exceeds 14×10^6 ° K. The emission measure $n_e n_i V$ has a constant value of about 1.4×10^{47} cm^{-3} both during an X-ray burst and from burst to burst. The solar X-ray bursts therefore differ mainly in the maximum temperature attained. A less detailed examination of later data shows that the phenomena we describe are not peculiar characteristics of a single active region.

I. INTRODUCTION

The OSO-III X-ray telescope, a collimated scintillation counter with spectrum analysis between 7.7 and 210 keV, has observed the Sun nearly continuously between March 9, 1967 and June 28, 1968. This paper provides a description of the data and their interpretation, and is based mainly on results during March 1967. A solar X-ray burst occurred 9 minutes after the instrument was turned on at 1059 U.T., March 9, and thousands of bursts have been observed since that time. The largest events generate X-rays with quantum energies greater than 210 keV. In contrast to this extreme, the Sun does not produce detectable fluxes of X-rays more energetic than 7.7 keV ($\lambda < 1.6$ Å) during quiet periods. Energetic solar X-ray bursts generally occur in conjunction with solar flares and the emission of radio waves. This X-ray emission represents a very small fraction of the energy flux radiated by the impulsive solar event, but the observation of the flux is essential for properly understanding the nature of the event.

Peterson and Winckler (1959) first observed hard solar X-rays with balloon-borne instrumentation, but between this time and the launching of the OGO (Orbiting Geophysical Observatory) and OSO (Orbiting Solar Observatory) satellites only a very few events were observed from rockets and balloons. Nevertheless, solar X-ray emission at longer wavelengths was known to be a common phenomenon from the work of the Naval Research Laboratories group (Friedman 1964) and from studies of ionospheric disturbances. Arnoldy, Kane, and Winckler (1968) reviewed the earlier hard solar X-ray observations and described those of the OGO-I and OGO-III satellites. The OSO-III data confirm most of their conclusions and suggest some new ones. The new results emerge

chiefly from the spectrum analysis, which had not previously been done extensively in this energy range, and from the ability of OSO-III to monitor the solar flux continuously for long periods of time. A brief account of some of the OSO-III observations has already been given (Hudson, Peterson, and Schwartz 1969*a*).

II. DESCRIPTION OF INSTRUMENT

Hicks, Reid, and Peterson (1965) have described the instrument and electronics in some detail. The detector consists of a NaI(Tl) scintillation counter, 5 mm thick by 9.57 cm^2 area, with an anticoincidence collimator whose angular response (FWHM) is 23°. The detector, which looks radially outward from the OSO wheel, scans the Sun and a great circle on the celestial sphere each 1.55-sec spin period. Each scan of the Sun yields an effective exposure of 1.0 cm^2 sec, with the absolute time of the observation determined within 2 sec, and successive scans are devoted to six differential and two integral energy channels. A complete readout of the energy spectrum requires 15.36 sec; this is the limiting time resolution of the observations. Table 1 lists these channels and the appropriate conversion factors. The factor 1.6×10^{-8} approximately converts counting rates in the (7.7–12.5)-keV channel into energy fluxes, ergs $(cm^2\ sec)^{-1}$, which for small events are approximately the integral fluxes above 7.7 keV.

Tape recorders on OSO-III store the data accumulated during an orbital period, permitting almost complete data coverage. However, the 550-km, 33° inclination circular orbit is such that occasional transits of the South Atlantic region of anomaly in the Earth's magnetic field occur, and the solar X-ray data are confused by the large fluxes of energetic charged particles. These gaps in the data, together with playback time of the tape recorder, occasional incomplete ground station coverage, and the 36-minute eclipse interval once each 96-minute orbital period, reduce the average data coverage to about 55 per cent.

Saturation effects appear in the data for large X-ray events whose peak flux exceeds 3×10^{-5} erg $(cm^2\ sec)^{-1}$ above 7.7 keV. For the purposes of this paper these events need not be discussed, although we shall describe two outstanding events in order to show the interrelationship of X-ray flux with other phenomena which are observed only in such major outbursts. The data that are saturated are partially recoverable, and we hope to present some of them in a later publication.

The Appendix describes the spectral response of the detector, the techniques used in verifying the calibration, and the background counting-rate spectrum.

III. SOLAR X-RAY DATA

At energies above 7.7 keV the solar X-ray flux is a transient phenomenon above the level of the equivalent background flux of the OSO-III instrument, 8×10^{-9} erg $(cm^2\ sec)^{-1}$ in the range 7.7–12.5 keV. At these energies the principal source of the background counting rate is the bright sky produced by the diffuse cosmic X-rays. A slowly varying component of solar X-radiation exists in addition to the X-ray bursts, but in this paper we shall concentrate on the bursts, specifically for the 2-week period March 9–23, 1967. The synoptic chart of Figure 1 summarizes the solar activity during this period, which was characterized by 2800-MHz daily flux values ranging from 127 to 156. The OSO-III X-ray telescope integrates the X-ray flux from the entire disk, and the only way to locate particular events is from their simultaneity with Hα flare listings. This technique, which has been much used in radio observations, is sufficiently accurate to show that certain active regions during this period of time were particularly important for X-ray production. McMath plage number 8740 produced many smaller bursts and also the major burst of March 22, 1967.

Five-hour segments of data, such as those shown in Figure 2, exhibit the slowly varying and impulsive components of the solar X-ray flux. The lower section of Figure 2

shows data on March 19, 1967, in which a clear day-night modulation proves the solar origin of the X-ray flux. The upper section, on May 11, 1967, does not show this modulation, and we therefore conclude that the slowly varying component of the solar X-ray flux was too weak to be detected on this date. X-ray bursts are seen on both days, although the bursts appearing in the May 11 data are extremely weak. The counting rate on the later date, exclusive of the bursts, is consistent with that expected from the diffuse source of the cosmic X-rays (Gould 1967).

TABLE 1

PROPERTIES OF THE DETECTOR

Channel Number	Discrimination Level	Exposure to Point Source	Exposure to Isotropic Flux (Day)	Exposure to Isotropic Flux (Night)	Background Rate
	Differential Channels				
	(keV)	(cm^2 sec keV)	(cm^2 sec sterad keV)	(cm^2 sec sterad keV)	(cm^2 sec sterad keV)$^{-1}$
2	7 7 12 5	4 8	1 8	11 1	42 ± 04
3	22	9 5	3 55	22 0	.125 ± 02
4	38	16	6 0	37 2	064 ± 010
5	65	27	10 1	62 2	.020 ± 005
6	110	45	16 9	105	010 ± 003
7	210	100	37.5	233	0058 ± 0013
	Integral Channels				
	(keV)	(cm^2 sec)	(cm^2 sec sterad)	(cm^2 sec sterad)	
1	7 7	1 0	375	2 32	
8	210	1 0	375	2 32	

A large X-ray burst (April 1, 1967, 0125 U.T.) observed by OSO-III appears in Figure 3 along with the associated radio burst. It is characterized by a fast rise of counting rate to a peak value, followed by a slower decay. The onset and decay portions of this time profile are approximately exponential functions of time. Because this shape is extremely common, and because its essential features are easily recognizable in the rare complex events, we shall discuss solar X-ray bursts in terms of its parameters: time to increase by a factor e ("rise time"), peak counting rate or flux, and time to decrease by a factor $1/e$ ("fall time").

The integral distribution function (Fig. 4) of peak fluxes of all 177 solar X-ray bursts studied during the 2-week interval falls off smoothly for larger events. The range of occurrence includes the minimum detectable burst (with a flux of 10^{-8} erg [cm^2 sec]$^{-1}$) and

bursts larger than the saturation level of the detector (peak flux in excess of 10^{-4} erg [cm^2 sec]$^{-1}$). Above a peak flux of 1.6×10^{-6} erg (cm^2 sec)$^{-1}$ the number of events larger than a given peak flux varies approximately inversely with peak flux. The distribution function below this flux level is modified by recognition effects which we will discuss in detail in a later section of the paper.

Distribution functions of the rise and fall times show peaks corresponding to most probable values. The average rise and fall times, for the first seventy-three bursts with peak fluxes greater than 1.6×10^{-6} erg (cm^2 sec)$^{-1}$ in the energy channel 7.7–12.5 keV, were 86 and 458 sec, respectively. There is no apparent correlation between rise time

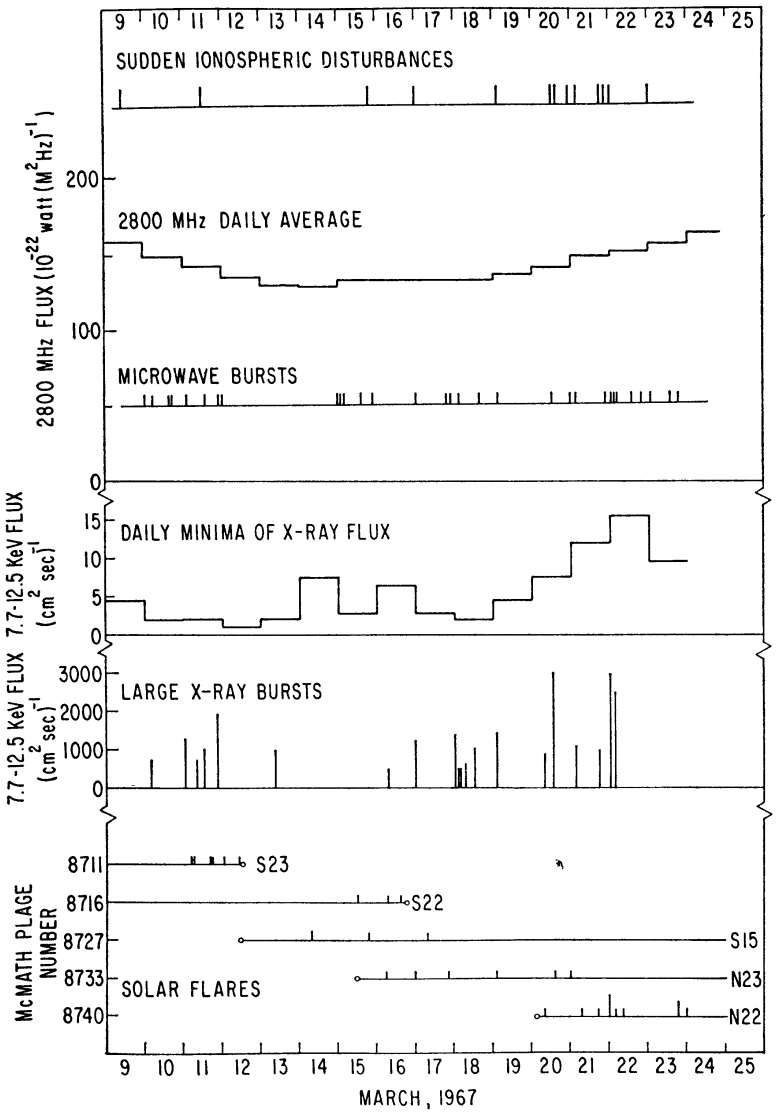

FIG. 1.—Phenomena which occurred during the first 2 weeks' operation of the instrument. Figure shows all the microwave bursts tabulated in the lists from Ottawa and Nagoya (excluding 0600–1100 U.T. intervals each day); all ionospheric disturbances listed in the CRPL Solar-Geophysical Data compilation; all solar flares from the same source (excluding subflares); and X-ray bursts exceeding a peak flux of 500 counts (cm^2 sec)$^{-1}$.

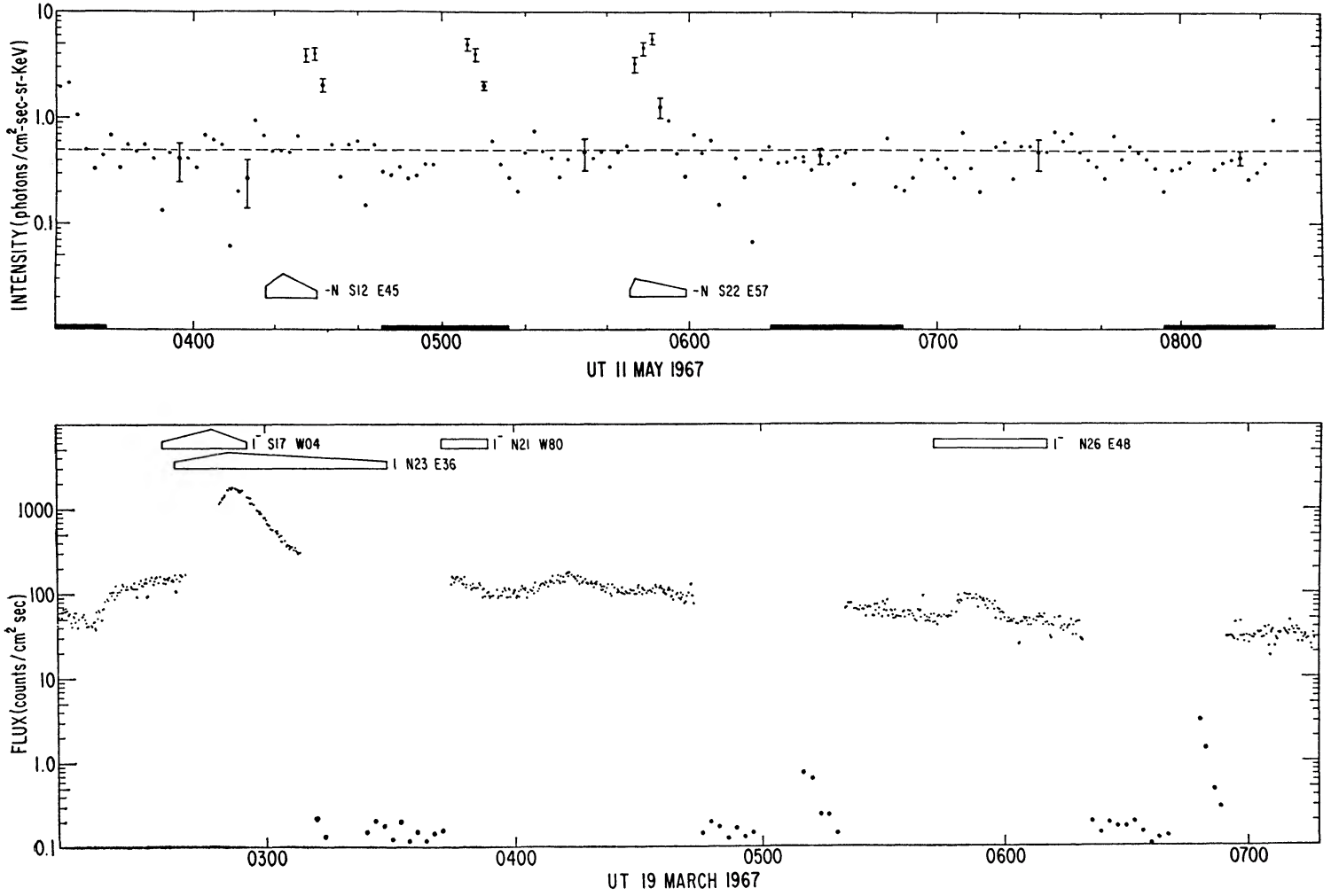

FIG. 2.—Representative counting rates, 7.7–12.5 keV, for a quiet period (*upper*) and an active period (*lower*). In the upper section the counting rates have been converted into intensities under the assumption that the source is isotropic, as is shown by the absence of a day/night modulation effect, and the dashed line represents the counting rate expected from the diffuse source of cosmic X-rays. Bars on the lower border show times of eclipse. The indicators of solar flares show the listed time of beginning, maximum, and ending.

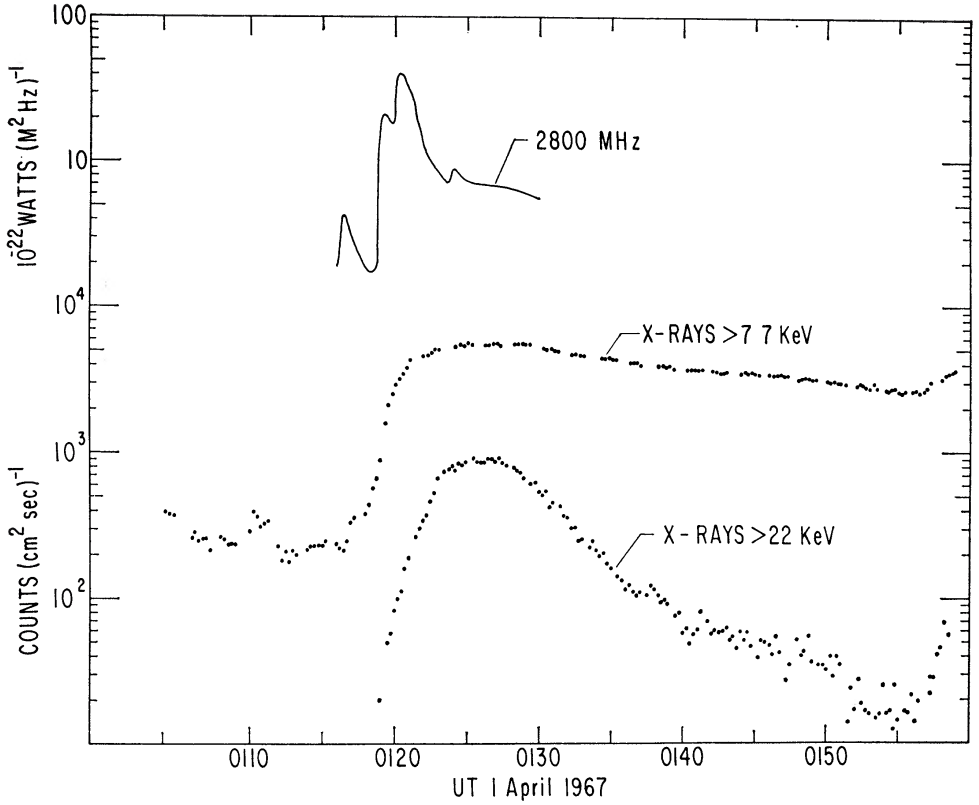

FIG. 3.—In this large X-ray burst the spectrum increased to a maximum hardness at about the time of maximum flux, and subsequently decreased smoothly. Decay time is longer than average. The impulsive microwave burst occurred simultaneously with the hard X-ray burst, and was followed by a postburst increase. A second event started at 0158.

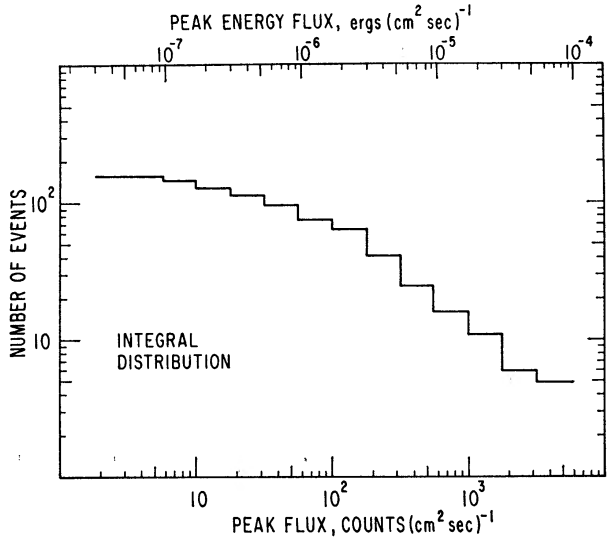

FIG. 4.—Integral distribution of peak fluxes, 7.7–12.5 keV, of X-ray bursts occurring during the first 2 weeks' operation of the instrument.

and fall time (Fig. 5) although there is a slight tendency for greater peak fluxes to be associated with faster rise times.

The spectrum of the X-ray emission depends strongly on the magnitude of the flux. The channel ratio of 12.5–22 keV to 7.7–12.5 keV counting rates (a measure of hardness related in the Appendix to the equivalent temperature of the emitting region) is almost proportional to the flux. At the beginning of a solar X-ray burst the flux increases rapidly, and at the same time the spectral hardness increases until the time of maximum flux is reached. The decay phase of each solar X-ray event consists of diminishing flux and de-

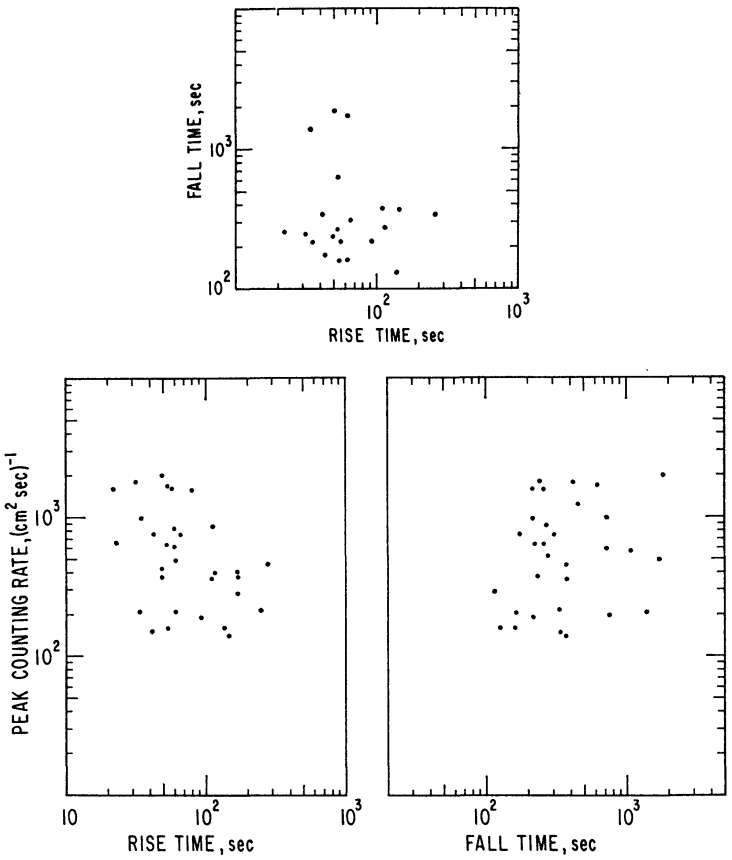

FIG. 5.—Correlation diagrams for the *e*-folding rise and fall times of (7.7–12.5)-keV X-ray flux and the peak fluxes in each solar X-ray burst. Although seventy-three events were used to make these diagrams, not all parameters were available for each event.

creasing effective temperature. The time profiles of the lowest two channels clearly show this effect, as for the event of March 18, 1967 (0228 U.T.), shown in Figure 6. If we plot the flux against the channel ratio as in Figure 7, the near proportionality of flux and spectral hardness manifests itself in the well-defined locus traced out by the instantaneous values. The information content in this graph is equivalent to that of the astronomical color-magnitude diagram, although the scales are approximately linear. The flux-spectrum proportionality is usually characterized by an asymmetry between the beginning and the end of an event; the spectrum during the onset is slightly harder than that during the decay at the same flux levels.

The maximum phases of many individual bursts define a similar locus on the flux-spectrum diagram. Each point in Figure 8 represents the flux and channel ratio of a solar X-ray burst at its time of maximum flux. Figure 8 shows that each solar X-ray

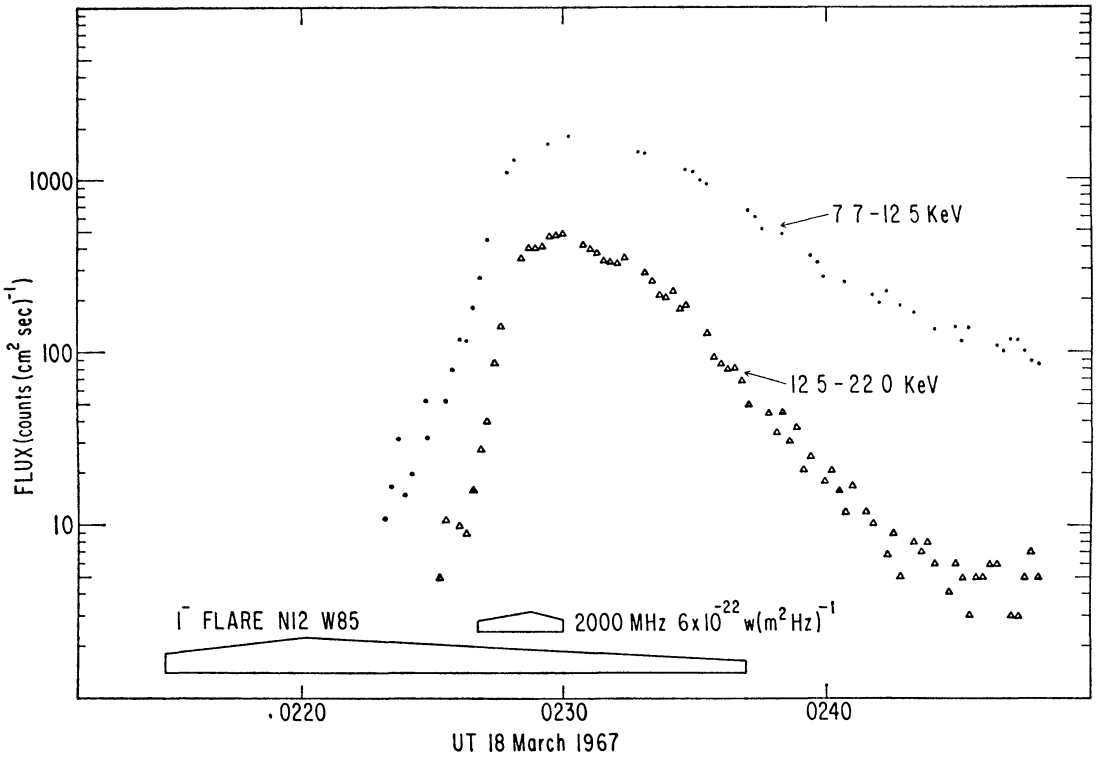

FIG. 6.—Time profile of the X-ray burst for which the spectral variations are displayed in Fig. 7. The small microwave burst and subflare probably associated with this event are indicated by symbols which give the times of beginning, maximum, and end.

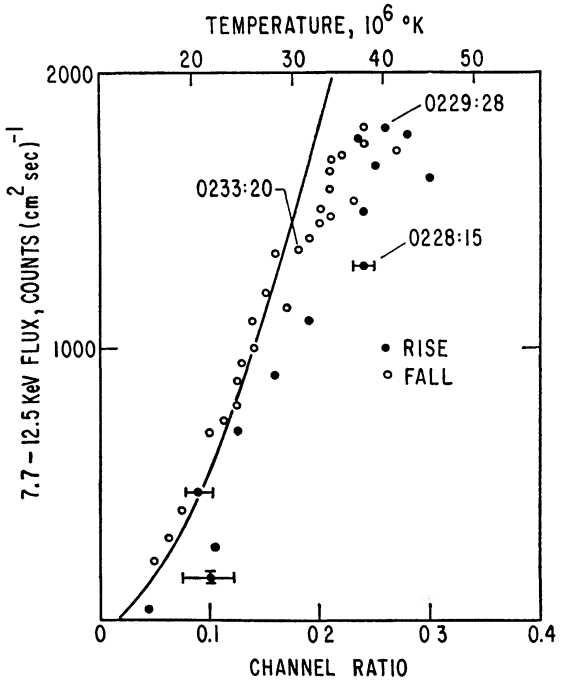

FIG. 7.—Diagram giving the correlation of instantaneous flux with channel ratio for the burst whose time profile appears in Fig. 6. The channel ratio, a measure of the hardness of the X-ray spectrum, is the ratio of (12.5–22)-keV to (7.7–12.5)-keV counting rates. The channel ratio determines the effective temperature, which is indicated in the upper scale. Filled and open circles represent, respectively, data from before and from after the time of maximum. Smooth curve represents the theoretical flux-temperature correlation for a source with constant emission measure $n_e n_i V = 1.4 \times 10^{47}$ cm^{-3}.

burst has very closely the same quantitative relationship between flux and spectral hardness or effective temperature. The nearly constant locus of the events may be interpreted in terms of a gas of constant emission measure $n_e n_i V$ reaching a different peak temperature for each event.

IV. MAJOR SOLAR X-RAY EVENTS

The largest and most energetic solar outbursts produce X-radiation as well as solar cosmic rays, ionospheric disturbances, Hα flares, and various kinds of radio noise. We shall discuss two such events (March 20, 1967, 1213 U.T., and March 22, 1967, 0036 U.T.) in detail in order to show the sequence of the various phenomena. These two events pro-

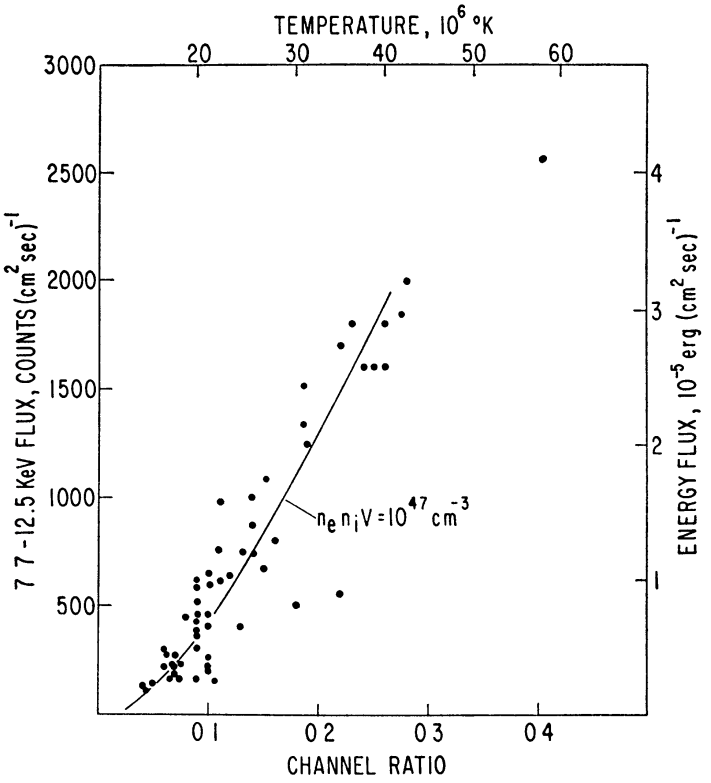

FIG. 8.—Diagram with the same kind of information as Fig. 7, except that each point represents the flux and channel ratio of a different X-ray burst, sampled at the time of maximum. Smooth curve represents theoretical locus of these points if each X-ray burst were characterized by the emission measure 1.0×10^{47} cm^{-3}.

duced the greatest solar X-ray emission observed by OSO-III in its first 2 weeks of operation, and they were selected for detailed discussion because extensive data existed on the related phenomena. In addition, Neupert *et al.* (1967), Neupert (1968), and Hall and Hinteregger (1969) have already described these events in terms of their soft X-ray and *EUV* spectra observed from OSO-III. These X-ray events were so intense (producing detectable fluxes of X-rays above 65 keV) that the OSO-III detector was saturated, and we will therefore only make qualitative statements about the data.

a) Event of 1213 U.T. March 20, 1967

A solar flare of importance 1^- began at 1159 March 20, 1967, and lasted until 1223 at S17W22 in McMath plage region 8727. At 2800 MHz a simple radio burst of 60×10^{-22}

W $(m^2\ Hz)^{-1}$ maximum flux occurred at 1202, followed by a postburst increase with peak flux 11×10^{-22} W $(m^2\ Hz)^{-1}$ at 1209. Another smaller simple burst followed at 1249. Still later multiple type III bursts occurred (at 1346.6–1348.4) with a type II burst at 1357.8–1401.2. Figure 9 shows these events and their time relationships along with the X-ray data.

OSO-III observed (7.7–12.5)-keV X-ray emission starting well before any of the other manifestations, including the ionospheric disturbances. The X-ray onset time was about 1135; the SID (Sudden Ionospheric Disturbance) started at about 1143, the optical flare at 1159, and the 2800-MHz emission at 1159. Enhanced emission of X-rays persisted until after 1500, with a major peak at 1213 and a smaller peak at 1405. The X-ray line emission tentatively identified with Fe XXV (Neupert *et al.* 1967) occurred with the microwave burst at the beginning of the event. The data in Figure 9 have not been corrected for dead time produced by the interaction of energetic particles with the anticoincidence shield, so that the 20-minute traversals of the radiation belts produced apparent minima in the counting rates at 1205 and 1340.

It is common to observe a gradual X-ray precursor as in this event; other examples from OSO-III are described by Hudson, Peterson, and Schwartz (1969*b*). On these occasions the soft X-ray flux provides the first indication that a solar event is going to occur. There are also instances in which the (7.7–12.5)-keV flux rises suddenly without a precursor. The onset time in the (7.7–12.5)-keV channel may precede the onset times of other phenomena, such as SID's, by as much as 10 minutes.

b) Event of 0036 U.T. March 22, 1967

A solar flare of importance 3^- began at 0013, March 22, 1967, at N24E69 in McMath plage region 8740. It reached its maximum phase at 0033 and ended at 0135. Strong radio emission accompanied the flare; the 3750-MHz emission showed two major peaks, the first occurring at 0032 (2750×10^{-22} W $[m^2\ Hz]^{-1}$), and the second at 0130 (2500×10^{-22} W $[m^2\ Hz]^{-1}$). Multiple type III bursts began at 0037, and type IV emission was observed from 0046.5 to 0100. The related ionospheric disturbance (SPA, Sudden Phase Anomaly) began at 0025 and lasted until 0530, with the maximum phase shift occurring at 0040. Figure 10 shows the chronological sequence of these events along with the OSO-III X-ray data.

The first X-ray emission preceded the very definite onset of the radio burst at 0025. The exact onset time of the X-ray burst could not be determined because OSO-III was in the Earth's shadow until 0017; when the satellite entered the shadow at 2341, the event had not yet begun. The X-ray onset time preceded the onset of ionospheric disturbance by at least 8 minutes, the fast drift bursts by at least 20 minutes, and the type IV emission by at least 30 minutes. The onset time of the X-ray flux probably coincided fairly closely with that of the optical flare at 0013. The X-ray flux rose exponentially with an *e*-folding time of approximately 130 sec at 10 keV, until 0025. Between 0025 and 0027 (at the time of onset of the radio burst) and flux increased very rapidly, and then more slowly until the peak at 0036, when type III radio bursts appeared. We will refer to the time of the sudden increase as the "flash phase" later. The line emission attributed to Fe XXV (Neupert *et al.* 1967) reached a maximum at about 0032, in better coincidence with the microwave burst than with the (7.7–12.5)-keV burst. The X-radiation persisted long after the disappearance of the optical and radio events, and showed no tendency to follow the time variations of the radio burst. The subsequent and larger 3750-MHz emission at 0130 occurred when the OSO-III was in the Earth's shadow, and therefore a detailed observation of a coincident X-ray burst was not possible. However, the data in Figure 9 suggest that, if a burst did occur, it was not proportionately as large as the burst at 0036. This X-ray event confirms the observation of Arnoldy *et al.* (1968), that the first microwave burst in a series is usually associated with X-ray production and that the succeeding bursts are not.

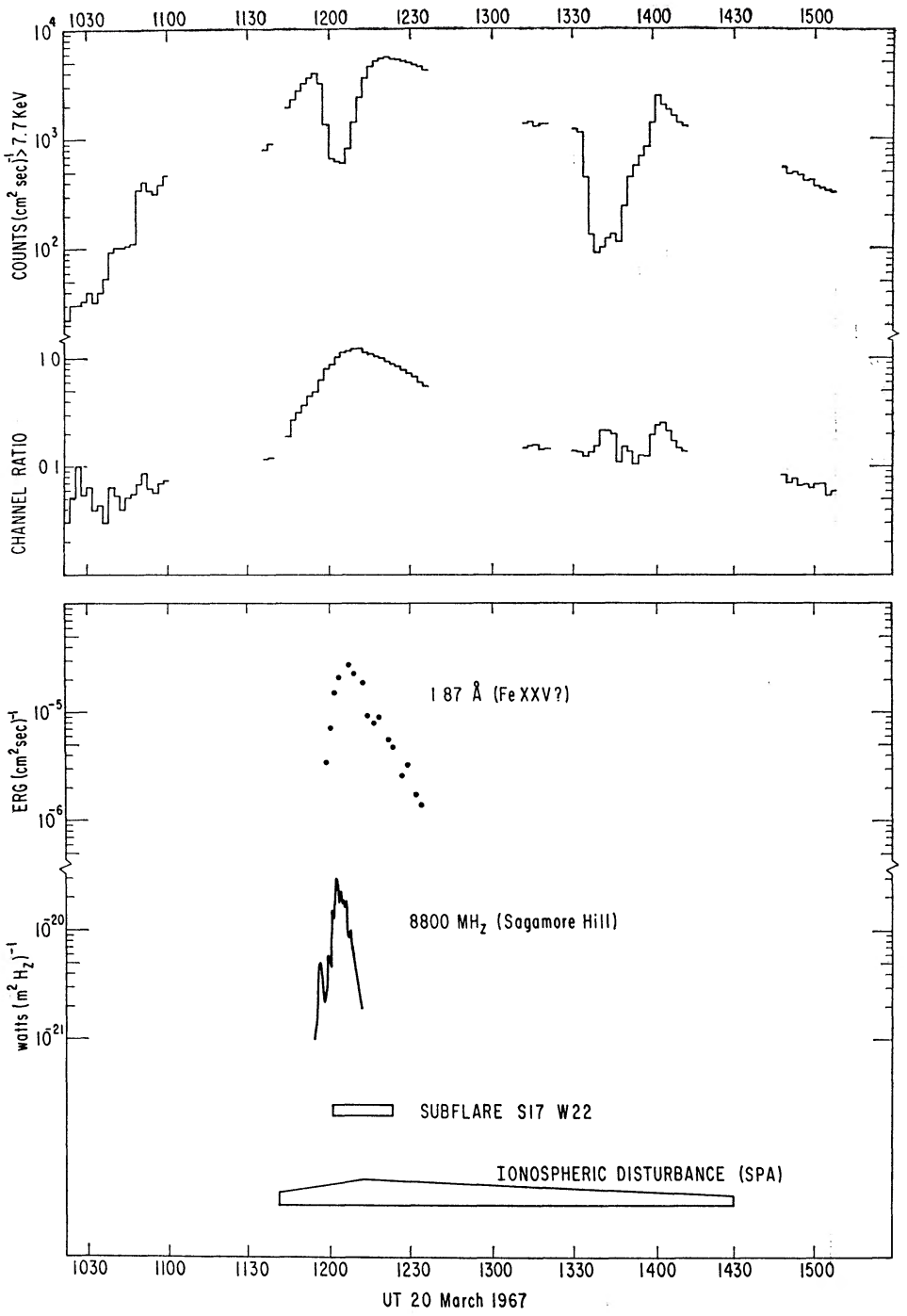

FIG. 9.—A major solar X-ray burst which was apparently associated with the subflare at S17 W22. Upper histogram is the time profile of the integral counting rate; lower histogram represents the variations of the channel ratio defined for Fig. 7. Dead time produced by radiation-belt particles caused the notches which appear in the time profile at 1205 and 1340 U.T. Lower section shows other data for comparison. Symbols indicate times of beginning, maximum, and end of the associated subflare and ionospheric disturbance (SPA).

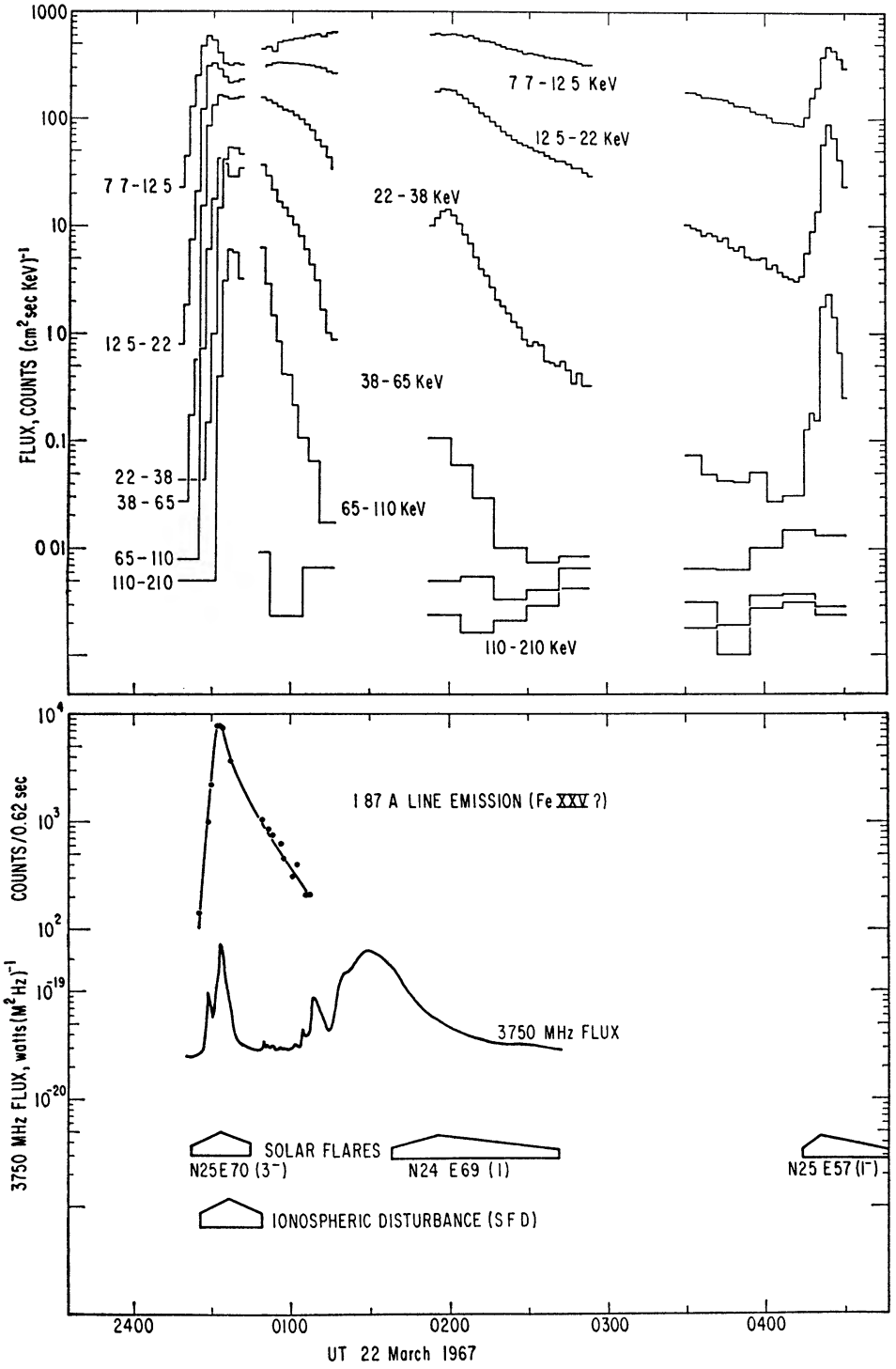

FIG. 10.—Largest solar X-ray burst observed during the first 2 weeks' operation of the satellite. Symbols indicate time of beginning, maximum, and end of the associated importance 3⁻ flare and ionospheric disturbance (SFD). Apparent decrease in flux between 0030 and 0130 in the lower channels is a spurious effect due to the saturation of the detector.

The microwave emission at 0130 was of spectral type IV (Kai 1967). This shows, at least for this single example, that the processes which create the type IV emission are not accompanied by as much X-radiation as are the processes responsible for other types of solar microwave emission. In the cases reported by Arnoldy *et al.* (1968), in which the hard X-radiation accompanied the first radio burst of a series, it seems likely that the radio events consisted of combinations of impulsive microwave outbursts (with X-rays) followed by type IV emission (without X-rays).

V. CORRELATION OF SOLAR X-RAY BURSTS WITH OTHER PHENOMENA

OSO-III provides a monitor with good time coverage for the detection of solar X-ray bursts in the energy range 7.7–12.5 keV. Previous monitoring has been done mainly at lower energies—for instance, with the ion chambers in the NRL Solrad satellite series (Friedman 1964). The statistics of the event correlations with solar radio emission, Hα flares, and SID's should therefore be of some interest in comparative studies of the occurrence statistics for X-rays of lower energy. White (1964*b*) and Teske (1968) show

TABLE 2

EVENT CORRELATIONS FOR 1967 MARCH 9–23

	Optical Flares (incl. Hα subflares)	Radio bursts (microwaves)	SID's (all types)	Type III radio bursts
Events without X-ray bursts	13	2	0	22
Events without coverage of X-radiation	184	31	2	42
Correlated events	96	25	10	10
X-rays without event coverage	35	71	....	75
X-rays without events	43	78	154	89
Event correlation	88%	92%	100%	31%
X-ray correlation	69%	24%	. .... .	10%

typical soft X-ray data and also discuss the occurrence statistics. Teske (1968) and Neupert *et al.* (1969) have described the soft X-ray detectors on OSO-III. We have not yet made detailed comparisons among the events simultaneously observed by these detectors.

The event correlations for the first 2 weeks of operation of OSO-III, 1967 March 9–23, are indicated in Table 2. We considered four types of events: Hα flares, microwave radio bursts, SID's, and spectral type III radio bursts. The table lists five categories of correlation for each type of event: (1) the occurrence of the event without the occurrence of an X-ray burst within a 10-minute time interval, (2) the occurrence of the event without sufficient X-ray data coverage, (3) simultaneous occurrence of the event and an X-ray burst within a 10-minute time interval, (4) occurrence of an X-ray burst without patrol coverage for the event, and (5) occurrence of an X-ray burst in the definite absence of the event. Two additional categories give the percentages of the correlations in either direction, excluding the events for which time coverage was not complete. The data in the table represent 174 X-ray bursts, 293 flares and subflares, 12 SID's, 58 single-frequency microwave bursts, and eighty-four spectral type III radio bursts. Figure 1 gives an overall view of the data during this interval.

Several recognition effects for X-ray bursts are important for the interpretation of these statistics. First, bursts of a given size may be obscured by larger bursts occurring at about the same time. This effect tends to reduce the number of small bursts recog-

nized. Second, small bursts can fit more easily into the gaps in the data coverage and thus not be recognized. Third, counting statistics at low flux levels tend to discriminate against small, rapid bursts. These effects are important in deciding whether a given event should be placed in category 1 (definite anticorrelation) or category 2 (insufficient data coverage). The thirteen category 1 events for Hα flares occurred when the slowly varying component of the solar X-ray flux was relatively large, and it may be that this enhanced background made it impossible to recognize the associated X-ray bursts. We did not try to correct the data in the table for any recognition effects in a quantitative way. Periods in which the (7.7–12.5)-keV X-ray flux exceeded about 200 counts $(cm^2\ sec)^{-1}$, as, for instance, for several hours after the event of March 22, 1967, were considered periods of no data coverage.

a) Solar Flares

Table 2 shows that the occurrences of Hα flares and solar X-rays are well correlated, a fact which was already well established by earlier rocket and satellite observations, and by balloon observations for the larger events. Considering only those instances in which there was adequate data coverage both in the Hα flare patrol and in the OSO-III data, 88 per cent of flares and subflares correlated with X-radiation, while 69 per cent of X-ray bursts correlated with flares listed in the *ESSA Solar-Geophysical Data* revised flare lists. This agreement of occurrence permits the conclusion that every Hα flare also produces X-radiation, although for some 12 per cent of flares the X-ray flux lies below the threshold of OSO-III sensitivity. Because the spectrum is correlated with the flux, the threshold of flux sensitivity corresponds to a fixed temperature, which is about 8×10^6 ° K for the OSO-III instrument. Thus 88 per cent of all flares and subflares produce a region hotter than this temperature, a completely unexpected result since such elevated temperatures are not required for the Hα emission.

For small solar events, X-ray observations by OSO-III have approximately the same sensitivity as the Hα observations. The X-rays do not suffer from decreased visibility for events occurring toward the limb because unit optical depth occurs well beneath the photosphere. If the X-ray source region is high in the solar atmosphere, then some fraction of events actually occurring around the limb will also be visible. The fact that category 5 (X-rays but no flares) of Table 2 is greater than category 1 (flares but no X-rays) may be partly due to this increased visibility of the X-ray source. We plan to correlate X-ray and Hα events as a function of longitude in order to determine the relative visibility versus central meridian distance.

The relationship between Hα flares and X-ray bursts is much more intimate than mere simultaneity of occurrence. For soft X-rays (Teske 1968), the details of the time structures may be very similar for the Hα and X-ray fluxes. In addition, there is a weak correlation between flare area and X-ray flux, as shown by Figure 11. The relationship between flare area and X-ray flux is also shown by an examination of the X-ray production in various importance classifications: Six importance 1 flares produced an average peak X-ray flux of about 800 $(cm^2\ sec)^{-1}$, while thirty-six subflares produced an average peak X-ray flux of about 310 $(cm^2\ sec)^{-1}$. However, the variability inherent in these correlations is illustrated by the fact that the very large X-ray burst of 1213 U.T., March 20, 1967, was associated with a subflare.

X-ray bursts frequently show a phase analogous to the flash phase of an Hα flare. Good examples of this sudden brightening during an X-ray burst are in the March 22, 1967, event (Fig. 10) and the March 23, 1967, event (Fig. 12), in both of which a gradual brightening preceded the sudden increase.

b) Single-Frequency Solar Radio Bursts

The fifty-eight radio bursts tabulated in Table 2 were derived from the lists of outstanding events from Ottawa, Penticton, and Nagoya, measured at various single

frequencies in the microwave range. The twenty-seven radio bursts for which there was X-ray data coverage accompanied solar X-ray bursts in all but two cases; the two failures both occurred on March 22, 1967, at times when the great 0036 U.T. event had not yet died away. Most of the radio bursts were classified as simple bursts, and none exceeded 60 flux units except for the March 22 event, which Covington (private communication) recorded at 1500 f.u.

Arnoldy *et al.* (1968) showed that every radio burst with peak flux greater than 80 f.u. at 3 or 10 cm was accompanied by a hard X-ray burst. The OSO-III data extend the range of correlations down to about 10 f.u. for the March 9–23, 1967, interval. Arnoldy *et al.* found a positive correlation between the peak radio flux of the impulsive microwave burst and the peak flux of hard X-rays. The degree of correlation observed on the OGO satellites was better for larger events. For the events small enough not to saturate the OSO-III instrument, we find that the ratio of radio energy flux to X-ray energy flux is

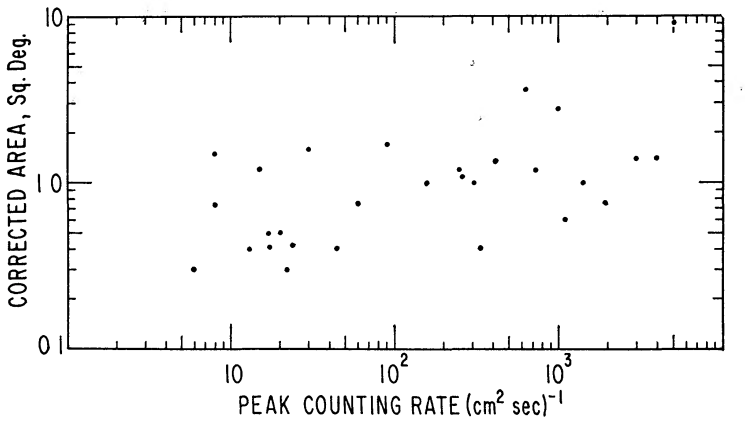

FIG. 11.—Correlation diagram of corrected flare area against peak counting rate, 7.7–12.5 keV, of the associated X-ray burst. This indicates that some parameter, such as temperature, is a more important indication of X-ray emission than Hα flare area or volume.

even more variable. The correlation of the radio and X-ray events is not as good for (7.7–12.5)-keV X-rays as for the higher-energy X-rays observed in larger events by the OGO ion chambers.

We may divide microwave bursts into two categories, fast and slow. The fast events are otherwise known as "impulsive bursts"; the slow events, as "gradual rise and fall" or "postburst increase" events. The (7.7–12.5)-keV X-ray flux also shows this clear distinction in time structures, although the X-ray flux tends to be more impulsive at higher energies and more gradual at lower energies, as typified by the event in Figure 12. Figure 13 shows a remarkable example of both impulsive and gradual correlated radio and X-ray bursts. The Hα flare listings suggest that both parts of the event originated in the same active region. The impulsive burst coincided with a small flare (importance 1); the gradual burst, with a large flare (importance 3$^-$). These events also afford a good example of the variability of the ratio of radio flux to X-ray flux at this energy. Although the source of the ~20-keV X-rays may be identified with the source of impulsive microwave bursts for the larger events (Arnoldy *et al.* 1968), a different relationship between the X-ray and radio emitters seems to be required for the softer X-ray production at or below 10 keV.

c) Sudden Ionospheric Disturbances

The flare-associated ionospheric disturbances are probably of more interest to ionospheric physicists than to astronomers. However, there is some information relating to

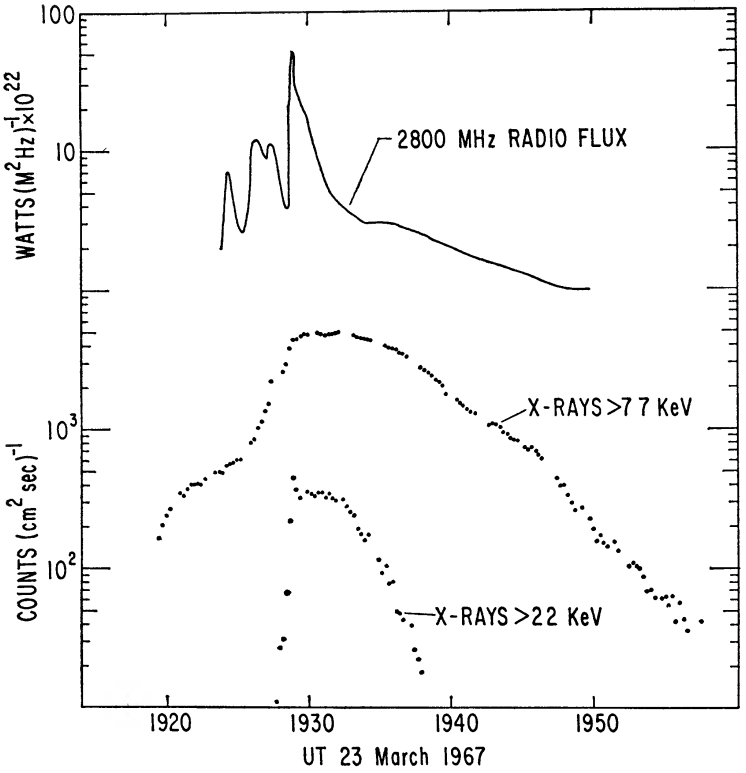

FIG. 12.—A large X-ray burst which exhibits a slow precursor increase followed by a rapid "flash" increase coincident with a microwave burst. Similar slow precursors occur in many solar X-ray bursts.

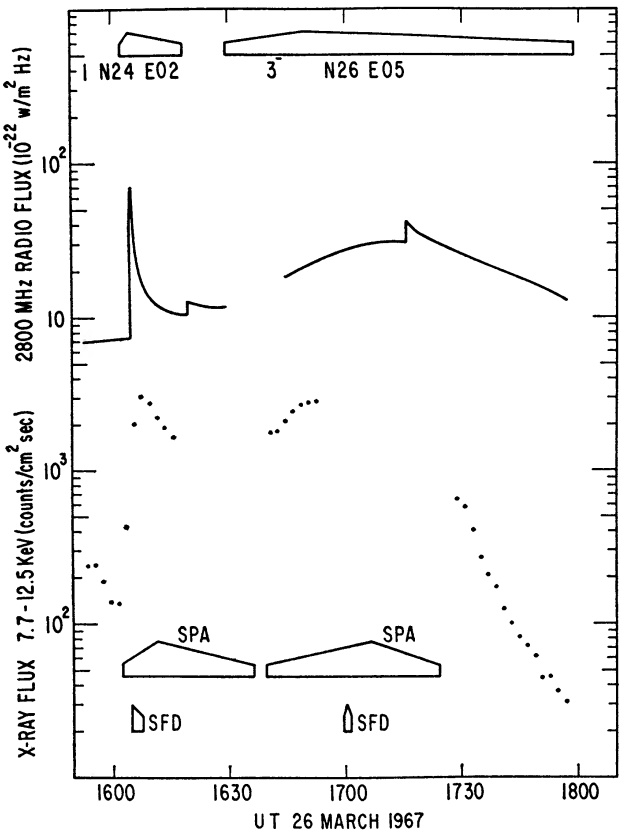

FIG. 13.—A remarkable example of an impulsive burst and a gradual burst occurring consecutively in the same active region. The optical counterpart of the gradual burst was a large flare, while the impulsive burst was associated with a smaller flare. The time profiles of the microwave burst were very similar to those of the X-ray bursts, but the ratio of X-ray flux to microwave flux changed during both bursts.

the energy spectrum of the solar emission that can be derived from a study of the occurrence of SID's. In particular, the disturbances of the ionospheric *F*-region (SFD, Sudden Frequency Deviation) must be due in part to solar ultraviolet radiation (Donnelly 1967), whereas the *D*-region disturbances (SPA) are due to harder solar emission. The ionosphere is not a very sensitive detector of solar emission of any wavelength, because every ionospheric disturbance during the period covered by Table 2 corresponded to a hard solar X-ray event that was quite large. Table 2 includes listings of all types of SID.

The details of time structure within single events may be summarized briefly as follows: The SPA peak phase shift is displaced to occur 4.1 minutes on the average later than the peak X-ray flux in the (7.7–12.5)-keV range. The recovery time for the SPA event is longer than that of the X-ray burst in the energy range 7.7–12.5 keV, and the time profile of the SPA does not tend to reflect small variations in the X-ray flux. These facts are consistent with the idea that the ionospheric processes have longer time scales than those of the energy source. Alternatively, the longer recovery time for SPA could be attributed to an origin in X-rays of lower energy than 7.7 keV. The softer X-rays have longer time scales and also tend not to reflect the rapid variations of the hard X-rays (Teske 1968). In this case, the delay of the SPA peak could be due in part to a delay in the time of maximum emission by the Sun of soft X-rays relative to the hard X-rays observed by OSO-III.

We have observed several instances of *F*-region disturbances (SFD) accompanying the flash phases of X-ray bursts. An example is the event of March 26, 1967, 1605 U.T. (Fig. 13). This phase of the X-ray burst is the time of maximum production of hard X-rays, and it is interesting that the ultraviolet flash may be exactly simultaneous with the X-ray flash. Friedman (1969) reports that the time of maximum of softer X-rays is generally later than that of harder X-rays in the several-angstrom range. It is remarkable that the ultraviolet flash may promptly accompany the hard X-ray flash while the intermediate-energy soft X-rays have a delayed and slower time scale.

d) Fast-Drift Radio Bursts

Type III radio bursts have their origin in streams of energetic electrons moving through the solar corona. The densities inferred for the regions where the fast electrons are observed are too small for appreciable X-ray production, although a relationship between the explosive processes producing the bursts at lower altitudes and the mechanism of X-ray production has been sought. The chromosphere is indeed related in some way to the type III burst phenomenon, as statistical studies (Malville 1962) have shown that flare occurrence in general and the flash phase of the flare in particular are strongly related to the type III burst. Table 2 shows that there is some tendency for X-ray bursts and type III bursts to occur simultaneously, although it is not so strong as for the other phenomena considered in Table 2. The weakness of the correlation shows that the Type III bursts are only a subsidiary part of the flare phenomenon. The time resolution of the OSO-III X-ray detector is not sufficient to determine whether the X-rays are associated with individual bursts or whether they are related to the burst group. Figure 14 shows an example of a type III burst associated with a fast, weak X-ray event. No Hα flare occurred at this time.

VI. THE NATURE OF THE SOLAR X-RAY SOURCE

a) The X-Ray Spectrum

The X-ray spectrum observed by OSO-III above 7.7 keV is probably due to the free-free and free-bound continua. Line emission (bound-bound transitions) is not important in this energy range (Neupert 1968). Other possible X-ray production mechanisms include the synchrotron and inverse Compton effects. The distinction between thermal

and non-thermal radiation has been historically important, although what is frequently termed "thermal" emission is not truly thermal because it is produced in an optically thin region. The "thermal" or quasi-thermal continuum arises from the free-free and free-bound transitions of a Maxwellian distribution of electron velocity, while the non-thermal continuum arises from the same X-ray production mechanisms in a non-Maxwellian distribution.

A good approximation (Elwert 1961) for the free-free continuum of an optically thin gas in which the electron distribution is Maxwellian, with temperature $T(^\circ\,\mathrm{K})$, electron and ion densities n_e and n_i (particles per cubic centimeter), is

$$I_\nu d\nu = 7 \times 10^{-41} g_{ff} d\nu \int \frac{n_e n_i}{(kT)^{1/2}} \exp\left(-\frac{h\nu}{kT}\right) dV \text{ ergs (cm}^2 \text{ sec)}^{-1}, \qquad (1)$$

where it is assumed that flux is detected at a distance of 1 a.u. from its source. The Gaunt factor g_{ff}, has been taken as unity in this work. The free-bound continuum has the same energy spectrum above the recombination edges, and its magnitude relative to the free-free component depends on the temperature as well as on the abundances of the elements.

The OSO-III covers a limited range of energies because of the steepness of the observed spectra, the limited dynamic range, and the problem of saturation. The examples in Figure 15 are two spectra from the burst of March 23, 1967, 1929 U.T. (the event shown in Fig. 12). The fit for the spectrum taken during the decay at 1942 U.T. is accurately matched by the computed response to a thermal spectrum corresponding to a temperature of $27 \times 10^6\,^\circ$ K. The error due to counting statistics is only about $1 \times 10^6\,^\circ$ K. The harder spectrum during the rise at 1928:15 U.T. is shown in comparison with the computed response for a power-law energy spectrum with index -2.6. Although thermal spectra may always be fitted to the data in the lowest two channels, the fit to three channels using a single temperature is not always as good as that shown in Figure 15. The rising spectrum of this event, as well as of most fast-rising events, is completely inconsistent with any simple thermal interpretation. An excess of high-energy photons is always observed.

An equivalent isothermal emitter for a given X-ray spectrum may be characterized by T and the emission measure, $n_e n_i V$. If the source is not an isothermal region, these quantities will vary with wavelength, but for that part of the spectrum for which $h\nu \geq kT$ the exponential dependence of flux on temperature makes the isothermal approximation valid. Most of emission comes from the region with the highest temperature. The appropriate range of temperatures for the OSO-III measurements at about 10 keV is $T \leq 10^8\,^\circ$ K, and in this range the numerical values for T and $n_e n_i V$ represent the temperature and emission measure of the hottest part of the plasma. The uncertainty about the contribution from free-bound emission makes the observed value of $n_e n_i V$ an upper limit.

The OSO-III observations show that $n_e n_i V$ is very nearly constant during the course of a solar X-ray burst (Fig. 7) and also that different X-ray bursts (Fig. 8) have approximately the same value, 1.4×10^{47} cm^{-3}. Almost all of the larger bursts lie in the interval $1\text{–}2 \times 10^{47}$ cm^{-3}. Solar X-ray bursts therefore differ mainly in the maximum temperatures that the source regions attain.

Earlier observations of the parameters $n_e n_i V$ and T for hard solar X-ray emission have been very sparse. The only other direct observations in the OSO-III energy range were those of Chubb, Kreplin, and Friedman (1966) of two bursts associated with importance 2^+ flares. At lower energies, proportional-counter spectrometers on the Ariel I satellite (Culhane *et al.* 1964), and on the OSO-IV satellite (Culhane *et al.* 1969) have also contributed relevant observations. Unfortunately, the extensive observations reported by Arnoldy *et al.* (1968) did not have spectral discrimination, and the measure-

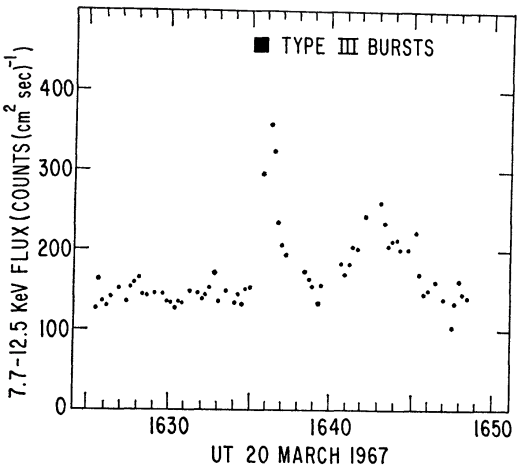

FIG. 14.—An example of the simultaneous occurrence of spectral type III radio bursts and a weak X-ray burst. No Hα flare or single-frequency radio burst was reported at this time. The X-ray bursts associated with type III emission are typically small ones.

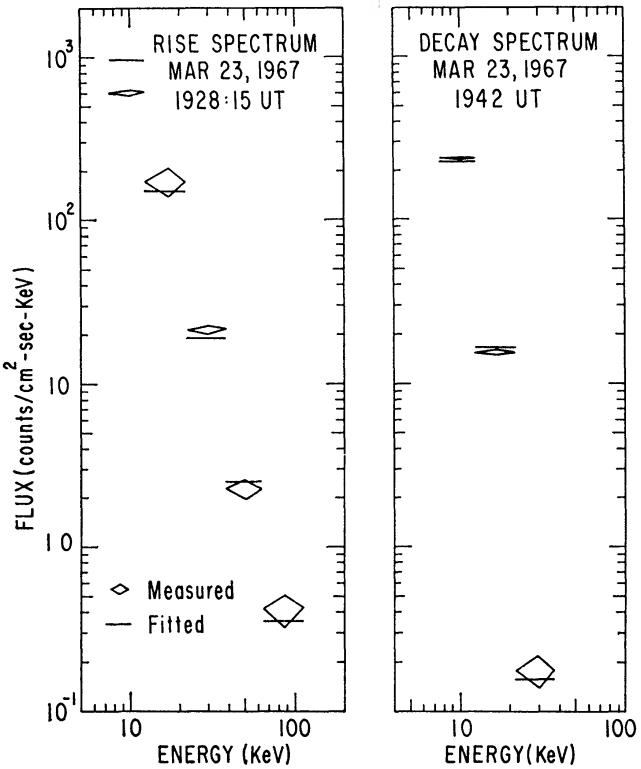

FIG. 15.—Two spectra from the event of Fig. 12, March 23, 1967. Left side shows data from 1928:15 U.T. in comparison with a power-law X-ray energy spectrum with exponent −2.6. Comparison spectrum was computed from the detailed spectral response of the detector. On the right side (1941:32–1943:34 U.T.) the comparison spectrum comes from a thermal model with $T = 27 \times 10^{6\circ}$ K, $n_e n_i V = 1.4 \times 10^{47}$ cm^{-3}.

ment of the flux at a single energy does not yield independent values for the effective temperature and the effective emission measure.

Chubb *et al.* (1966) observed two X-ray bursts in the range 20–100 keV with scintillation-counter spectrometers. These detectors were carried on sounding rockets which were launched at the times of Hα flares of importance 2+ (August 31, 1959, 2252 U.T., and September 1, 1959, 1702 U.T.). The spectra appeared thermal in origin, and Table 3 gives the observed values of emission measure and temperature. The agreement of the values for emission measure between these observations and those of OSO-III 8 years later is good for the September 1 flare and poor for the August 31 flare. The September 1 flare was observed during the time of maximum X-ray emission, and the emission measure increased while the flux increased, reaching a maximum value which remained relatively constant. This temporal behavior is similar to that observed in the OSO-III data (shown, for instance, in Fig. 7).

The proportional-counter observations yield parameters for the X-ray continuum emission which should be directly comparable with the OSO-III results, provided that the relative importance of line emission is understood. The Ariel-I observations (Culhane *et al.* 1964) covered the energy range 1–2.5 keV (5–12 Å). The flare spectra proved to be harder than those from quiet times, implying a higher temperature in the active region during the X-ray burst. A flare on April 27, 1962 (2300 U.T.) was found to have an emission measure $n_e n_i V = 6 \times 10^{47}$ cm^{-3}, whereas non-flare emission was characterized by an emission measure 3×10^{48} cm^{-3}. The same observers have operated an improved proportional-counter spectrometer system on OSO-IV (Culhane *et al.* 1969). The new instrument thoroughly covered the energies below 12 keV with a time resolution of 15 seconds and was calibrated in flight. These observations, which also give an emission measure of 10^{47} cm^{-3}, may not be directly comparable with those of OSO-III since they pertain to an active region not in the flaring state rather than to the flare itself. The OSO-IV does, however, observe elevated temperatures during solar flares.

TABLE 3

DIRECT OBSERVATIONS OF EMISSION MEASURE $n_e n_i V$

Date	Time (U T)	Condition	Emission Measure (cm^{-3})	Energy Range (keV)
1959 August 31	2252	Flare	1 7×10^{46}	20–50
1959 September 1.. .	1702	Flare	0 1-1 5×10^{47}	40–100
1962 April 27 .	2300	Flare	6×10^{47}	1–2 5
1962 April 27... .	.... ..	Quiescent	3×10^{48}	1–2
1967 December 9 . .	0009	Quiescent	1×10^{47}	2 5–8

In summary, the other observations of the hard solar X-ray flux have yielded values for the parameters of the continuum emission which are consistent with those derived from the OSO-III. If the constancy of emission measure required by the OSO-III does persist, the discrepancies which are seen in Table 3 may reflect the differences in instrumentation and data-handling techniques. The modern value for the emission measure is very different from that inferred from earlier measurements in narrow energy windows at lower energies (White 1964*a*). Without spectral information, ambiguity exists between sets of values of temperature and emission measure. The choice of coronal temperatures of about 2×10^6 ° K led to estimates of the emission measure on the order of 10^{50}, which is also consistent with that of the entire corona. The later data show that this estimate was about three orders of magnitude too large and that production of the harder X-rays is concentrated in the active regions at high temperatures.

b) Time Scales

The formula for free-free emission from a thermal plasma leads to some simple conclusions which are valid when thermal conditions prevail, such as during the decay phases of solar X-ray bursts. A change in the X-ray flux must be due either to a change in the temperature or to a change in the emission measure. The OSO-III data show that the emission measure is approximately constant during a burst. Therefore, the time structure of the burst at a given X-ray energy exactly reflects the time structure of the temperature changes within the emitting region, and thus of the energy content of the region in thermal particle motions. The interval of increasing X-ray flux corresponds to energy input into the radiating plasma or the duration of the acceleration mechanism, and the period of decreasing X-ray flux indicates that the energy input is either small or non-existent.

Coulomb collisions play an important role in the theory of the heating and cooling of the flaring region. Without being specific about the details of a model, we can say at least that the acceleration mechanism produces a non-Maxwellian electron spectrum which must relax into a Maxwellian spectrum. The electron-electron collisions bring about this thermalization, and, if the resulting electron temperature differs from the local ion temperature, a slower relaxation, due to electron-ion collisions, restores mutual equilibrium. The latter process is slower by approximately the ratio of electron mass to proton mass (Spitzer 1962). The exact formulas for the electron-electron relaxation are model dependent. For the model of Takakura and Kai (1966), in which a small fraction of the electron population is excited and then relaxes back into a normal coronal temperature, we have

$$\tau_{ee} = \frac{5 \times 10^{-38}}{n_o} \frac{v^5}{T_6} \text{ sec} \tag{2}$$

for the energy exchange characteristic time, where v is the electron speed in centimeters per second, T_6 is the temperature (in millions of degrees Kelvin) of the ambient electrons, and n_o is the ambient electron density per cubic centimeter. If the energy is comparable to kT, or if the number of electrons that are accelerated is not a small fraction of the whole population, then

$$\tau_{ee} = \frac{6.96 \times 10^6}{n_o} T_6^{3/2} \text{ sec} \tag{3}$$

is a more accurate formula. If the effective temperature is observed to vary more rapidly than the energy exchange time, the electron distribution cannot be Maxwellian. For instance, in the X-ray burst of 0230 U.T., March 18, 1967 (Fig. 6), the effective temperature increased by about a factor of 2 in about 60 sec. This is just equal to the electron-electron energy exchange time for a density of 6×10^9 cm^{-3} and an ambient temperature of 2×10^6 ° K. Therefore, the electron distribution should be non-Maxwellian, and in fact the X-ray spectrum was systematically harder during the rising phase of the X-ray burst than during the decay. Figure 7 illustrates the magnitude of this spectral asymmetry.

The possible cooling mechanisms include not only the Coulomb collisions of electrons with ions, but also ionizing collisions, synchrotron damping, and possible escape of the fast electrons from the dense region where the X-rays are produced. Appreciable escape is probably ruled out by the observed constancy of the emission measure. Takakura and Kai (1966) have shown that synchrotron damping can be an important factor in the decay of the event, and can of course produce the impulsive microwave radio bursts. It is therefore not clear to what extent the collisional processes (including wave-particle interactions) are important. The decay times are of the right order of magnitude to

account for the decrease in terms of collisions of fast electrons with slow ions alone. For example, an X-ray burst observed on April 5, 1967, at 0740 U.T. had an effective temperature of 2.1×10^7 ° K and a very fast decay time of about 180 sec. From the formula for electron-ion energy exchange time, these values determine the density as 6×10^9 ions cm^{-3}. Slower events suggest densities as low as about 5×10^8 ions cm^{-3}, but these values can only be regarded as upper limits because of the uncertainty as to which loss mechanisms are important. The electron-proton collisions are not an important loss mechanism if the proton temperature is comparable to the electron temperature.

c) The Size and Location of the X-Ray Source

Assuming a value for the density, we may compute the volume of the X-ray emitting region from the emission measure. For a density 10^9 cm^{-3} we find 1.4×10^{29} cm^3. For a spherical gometry, this corresponds to a diameter of 5.2×10^4 km, which is the size of a large flare. The calculation is sufficiently uncertain so that we may only say that the X-ray emitting volume is comparable in size to the Hα flare. Because the same value of emission measure holds true for X-ray bursts associated with subflares, it is fairly certain, in these cases at least, that the X-ray volume is not smaller than the Hα volume. The variability of decay times of X-ray bursts suggests that the densities within the sources are also variable and therefore that the sizes of different X-ray sources may also be different. High-resolution X-ray photographs of the Sun (Underwood and Muney 1967) also show sources of different sizes. The constancy of emission measure requires only that $n_e n_i V$ be the same for each X-ray region.

The changes of emission measure during the evolution of an X-ray burst provide information about the expansion of the X-ray emitting volume. If the medium is fully ionized and no appreciable recombination takes place, then $n_e n_i V$ should vary as V^{-1}. Under these conditions, the constancy of the emission measure means a constant volume. Expansion of the active volume results in a decreasing emission measure. In most of the X-ray bursts, changes in $n_e n_i V$ are less than about a factor of 2, including the great X-ray burst associated with importance 3$^-$ flare of March 22, 1967. On this occasion the detector was saturated for about 2 hours during the time of maximum flux, but a comparison of the emission measures before and after the maximum showed an increase of about 60 per cent at a temperature of 25×10^6 ° K. Such an increase in emission measure suggests a decrease in volume or compression. We have previously interpreted this typical increase in effective emission measure as a change in the nature of the spectrum from non-thermal to thermal. Whether the observed slight increase is a spectral effect or evidence for compressive motion of the radiating volume cannot be decided until more is known about the physical parameters of the region.

If the X-ray source exhibits no motion, or if its motion is such that $n_e n_i V$ is always maintained a constant, then it is difficult to associate it with solar phenomena which exhibit obvious large-scale motions: Hα flares frequently emit surges or sprays into the corona; radio observations indicate the presence of moving coronal clouds; and solar electrons are frequently directly detected at the distance of the Earth's orbit promptly following a solar flare. Arnoldy *et al.* (1968) and Lin (1968) have established the close connection between the occurrence of solar electrons and emission of hard X-rays. Apparently we must divide the energetic electrons existing in the solar-flare region into two populations, one of which remains stationary in the lower corona and emits the X-radiation observed by OSO-III.

VII. SUMMARY

This description of the OSO-III data on solar X-rays has been based mainly on the 174 solar X-ray bursts detected in the first 2 weeks of operation of the satellite, with some examples drawn from the later data. We have examined sufficient data to be sure

that the following conclusions are not peculiar to a single active region, although the data sample was not extensive enough to permit a study of the solar cycle variation of the phenomena.

1. Hard solar X-radiation accompanies solar flares and subflares (88 per cent correlation for 109 events), microwave bursts (92 per cent of twenty-seven events), and sudden inonospheric disturbances (100 per cent of 10 events), and is usually the first warning of a solar event.

2. The correlation with type III radio bursts (31 per cent of thirty-two events) is not as good, although there is still a definite positive correlation. Probably this weakness of correlation is not due to the relative sensitivities of the detection techniques, but indicates that the two phenomena are not part of the same physical mechanism.

3. The X-ray spectrum is non-thermal at the beginning of an impulsive X-ray burst but essentially thermal during the decaying phase.

4. The average *e*-folding rise time for X-ray bursts in the (7.7–12.5)-keV range is 86 sec, and the average *e*-folding fall time is 458 sec.

5. The electron temperatures in the X-ray emitting regions often exceed 5×10^7 ° K, with about 88 per cent of flares and subflares generating temperatures greater than 8×10^6 ° K.

6. The emission measure $n_e n_i V$ is constant both during a single burst and from burst to burst, and its value is about 1.4×10^{47} cm^{-3}. The differences in the observed peak X-ray fluxes are mostly due to differences in the maximum temperatures attained during the events.

7. The constancy of the emission measure may be taken as evidence that there is no appreciable expansion of the X-ray emitting plasma during the course of the X-ray burst.

8. The decay times of the bursts yield upper limits on the ion density of 10^9–10^{10} cm^{-3}.

9. The total energy of the X-ray emitting region for a subflare exceeds 2×10^{29} ergs.

The OSO-III data show that the main energy input during the flare process is limited to the initial or flash phases of the event, and that during this energization the electron-distribution function is non-Maxwellian. A description of the spectral variations in this phase will provide the essential information needed to identify the acceleration mechanism and the source of the solar-flare energy, a significant portion of which resides in the plasma which produces the hard solar X-radiation. Another field of investigation which will be very fruitful is the detailed statistical study of the X-ray production in relation to other forms of solar emission; the close similarity of Hα and X-ray light curves is a striking and unexplained fact. The history of X-ray production of a particular active region may provide some help in understanding its growth and decay. The OSO-III data will give opportunities for preliminary study of some of these questions, but others will require new instrumentation with better dynamic range, resolving power (Vaiana *et al.* 1968), and time coverage.

The authors gratefully recognize the contributions of many individuals and organizations who have made the OSO-III possible. The University of California, San Diego, X-ray telescope was designed, constructed, and integrated in the spacecraft by Messrs. Donald Hicks and Lou Reid of the Ball Brothers Research Corporation, where the satellite itself was also constructed and qualified. The OSO-III would not have occurred without the efforts of the late Dr. John C. Lindsay and Mr. L. T. Hogarth of the Goddard Space Flight Center. Discussions with many scientists have contributed to the clarification and interpretation of this data. A. E. Covington and J. P. Castelli generously provided copies of the radio records for several events. Finally, many members of the UCSD X-ray astronomy group have contributed to the instrument design, tests, and data reduction over the past 5 years. This research was supported under contracts NAS5-3177 and NsG-318 through the National Aeronautics and Space Administration.

APPENDIX

I. DETECTOR SPECTRAL RESPONSE

A scintillation counter converts a monoenergetic input X-ray spectrum into a pulse-height distribution that is approximately Gaussian. For the OSO-III detector this distribution has a standard deviation of 2.3 keV (85 per cent FWHM) at the ^{55}Fe X-ray energy of 5.9 keV. Other factors in the operation of the detector, such as K X-ray escape, efficiency, and window transparency, must also be considered, but the finite width of the monoenergetic pulse-height distribution and the steepness of the natural spectra provide the main difficulty in deducing the solar X-ray spectrum from the observed counting-rate spectrum. The most practical way to relate the solar spectrum to the observed spectrum is to make comparisons with the computed response of the detector to various model spectra. The pulse-height distribution produced by a spectral energy flux $F(h\nu)$ ergs (cm^2 sec erg)$^{-1}$ is

$$P(E)dE = dE\int_0^\infty F(h\nu)\epsilon(h\nu)\,\exp\left[-(E-h\nu)^2/2\sigma^2(h\nu)\right]/\left[(2\pi)^{1/2}h\nu\sigma(h\nu)\right]dh\nu\,. \quad (4)$$

This formula explicitly shows all of the effects used in model-spectrum calculations except for the K X-ray escape correction (Lidén and Starfelt 1953). The standard deviation of the pulse-height distribution is $\sigma(h\nu)$, and $\epsilon(h\nu)$ is the detector efficiency, including window transparency. The standard deviation of the monoenergetic pulse-height distribution was assumed to vary as $(h\nu)^{1/2}$. The formulae of Lidén and Starfelt yield an escape probability for K X-rays of 21 per cent at 34 keV, above which energy the escape probability falls off approximately exponentially with an e-folding energy of 36 keV. For the steep spectra which are most important for the results discussed in this paper, the escape corrections are negligible.

The spectrum of free-free transitions in an optically thin medium, but with a thermal distribution of electron velocities, is approximately of the form (Spitzer 1962)

$$F(h\nu) = \text{const.}\,\exp\left(-h\nu/kT\right)/\sqrt{(kT)}\ \text{ergs (cm}^2\ \text{sec erg)}^{-1}\,, \quad (5)$$

where T is the temperature. This formula is not strictly correct because it assumes that the average Gaunt factor is unity; actually, solar conditions require a more precise calculation valid for high-Z materials and relativistic temperatures. The approximate formula was used to generate the curves shown in Figure 16, which characterize the temperature of the radiating plasma as functions of the spectral ratios of adjacent channels of the pulse-height analyzer. The numbers on the curves in Figure 16 identify the energy channels, which are described in Table 1. Other comparison spectra have been generated, for instance, from power-law X-ray spectra.

II. THE DETECTOR BACKGROUND

The Sun fills only a small part of the aperture of the telescope, and the diffuse component of the cosmic X-rays is responsible for most of the background counting rate, at least at lower energies. Above about 100 keV the secondary γ-rays from the high-energy primary cosmic radiation begin to form the main contribution to the background counting rate. The exposure to the Sun is 1.0 (cm^2 sec) per readout (this is computed from the spin rate, the angular response function of the telescope, and the 0.25-sec duration of the data accumulation), and the exposure to an isotropic background is 0.4 (cm^2 sec sterad) per readout. The background rate is occasionally increased by the presence in the aperture of discrete sources of cosmic X-rays or of light from the Earth. The detector has frequently been used for cosmic X-ray observations from balloons, and so there is considerable information about the origin of that component of the background spectrum due to secondary production from the charged-particle cosmic rays (Hicks *et al.* 1965; Peterson, Jerde, and Jacobson, 1967). Figure 17 and Table 1 show the OSO-III background

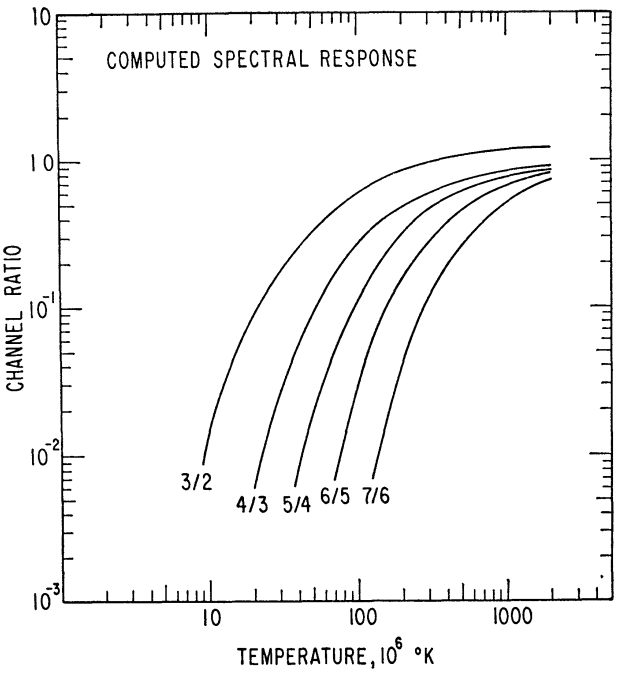

FIG. 16.—Spectral ratios of adjacent channels according to the thermal interpretation of the spectrum, computed from the detailed spectral response of the detector. Numbers beside each curve give the energy channels identified in Table 1.

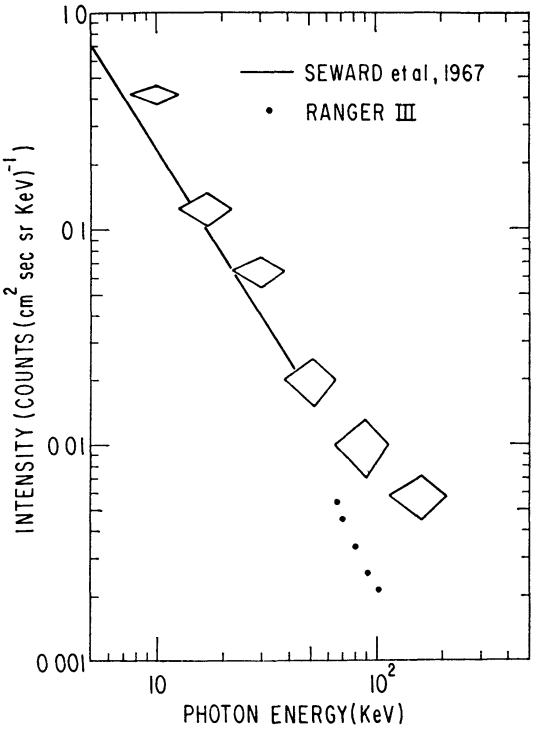

FIG 17.—A background counting-rate spectrum observed on May 11, 1967, at about 0730 U.T. The (7.7–12.5)-keV counting rates for this time also appear in Fig. 2. Neither Earth nor any known discrete sources of cosmic X-rays were in the telescope aperture. Straight line represents the data of Seward *et al.* (1967); dots represent the Ranger III data (Metzger *et al.* 1964).

spectrum when there were no contributions from discrete cosmic X-ray sources or Earth albedo. Solar X-ray emission must have also made a neglectable contribution to the background rates at this time.

Peterson (1965) described the activation of detectors containing iodine by the intense particle fluxes in the Earth's radiation belts. The counting rates produced by this activation (β-decay from ^{128}I with a half-life of 25.6 minutes) are negligible in comparison with the other sources of the counting-rate background.

III. CALIBRATION OF THE DETECTOR

OSO-III does not provide a direct calibration of the detector against a radioactive source, so it is necessary to rely on indirect means of calibration. We have used two techniques: the observation of "known" spectra, and the monitoring of the integral counting rate above 210 keV.

The "known" spectra were those of the diffuse cosmic X-ray sources (Seward *et al.* 1967; Metzger *et al.* 1964) and the Crab Nebula (Peterson, Jacobson, and Pelling 1966), sources which are not considered variable. The OSO-III observations agree within a factor of 2 with the previously reported values for each (Gould 1967), but unfortunately the other measurements are hardly more accurate than this. The Crab Nebula calibrations came in early June 1967, after 3 months' operation of the detector. The diffuse component has been observed continuously, and these measurements establish the gain change to have been less than 20 per cent.

The integral counting rate (> 210 keV) is due indirectly to the charged cosmic-ray beam and so should be constant at a given geomagnetic cutoff. The data show this counting rate to be constant within about 20 per cent for the first three months of operation. This is interpreted to indicate that the gain of the instrument was stable over this period.

REFERENCES

Arnoldy, R. L., Kane, S. R., and Winckler, J. R. 1968, *Ap. J.*, **151**, 711.
Chubb, T. A., Kreplin, R. W., and Friedman, H. 1966, *J. Geophys. Res.*, **71**, 3611.
Culhane, J. L., Sanford, P. W., Shaw, M. L., Pounds, K. A., and Smith, D. G. 1969, *Space Research* (to be published).
Culhane, J. L., Willmore, A. P., Pounds, K. A., and Sanford, P. W. 1964, *Space Research IV*, ed. P. Muller (Amsterdam: North-Holland Publishing Co.), pp. 741–758.
Donnelly, R. F. 1967, ESSA Technical Report IER 19-ITSA 19.
Elwert, G. 1961, *J. Geophys. Res.*, **66**, 391–401.
Elwert, G. 1964, in *AAS-NASA Symposium on the Physics of Solar Flares* (Washington: Scientific and Technical Information Division, NASA), p. 365.
Friedman, H. 1964, in *AAS-NASA Symposium on the Physics of Solar Flares* (Washington: Scientific and Technical Information Division, NASA), p. 147.
———. 1969, *Space Research* (to be published).
Gould, R. J. 1967, *Am. J. Phys.*, **35**, 376.
Hall, L. A., and Hinteregger, H. E. 1969, *Space Research* (to be published).
Hicks, D. B., Reid, L., Jr., and Peterson, L. E. 1965, *IEEE Trans. Nucl. Sci.*, **NS-12**, 54–65.
Hudson, H. S., Peterson, L. E , and Schwartz, D. A. 1969*a*, *Solar Physics*, **6**, 205.
———. 1969*b*, *Space Research* (to be published).
Kai, K. 1967, Proc. *A S.A.*, **1**, 49.
Lidén, K., and Starfelt, N. 1953, *Ark. f. Fys.*, **7**, 427.
Lin, R. P. 1968, *Canadian J. Phys.*, **46**, S757.
Malville, J. M. 1962, *Ap. J.*, **135**, 834.
Metzger, A. E., Anderson, E. C., Van Dilla, M. A., and Arnold, J. R. 1964, *Nature*, **204**, 766.
Neupert, W. M. 1968, *Ap. J. (Letters)*, **153**, L59.
Neupert, W. M., Gates, W., Swartz, M., and Young, R. 1967, *Ap J. (Letters)*, **149**, L79.
Neupert, W. M., Swartz, M , White, W. A., and Young, R. M. 1969, *Space Research* (to be published).
Peterson, L. E. 1965, *J. Geophys. Res.*, **70**, 1762.
Peterson, L. E., Jacobson, A. S., and Pelling, R. M. 1966, *Phys. Rev. Letters*, **16**, 142.
Peterson, L. E., Jerde, R. L., and Jacobson, A. S. 1967, *AIAA Journal*, **5**, 1921.
Peterson, L. E., and Winckler, J. R. 1959, *J. Geophys. Res.*, **64**, 697.

Seward, F., Chodil, G., Mark, Hans, Swift, C., and Toor, A. 1967, *Ap. J.*, **150**, 845.
Spitzer, Lyman. 1962, *The Physics of Fully Ionized Gases* (2d ed.; New York: Interscience Publishers).
Takakura, T 1960, *Publ. Astr. Soc. Japan*, **12**, 325.
Takakura, T , and Kai, K. 1966, *Publ. Astr. Soc. Japan*, **18**, 57.
Teske, R G. 1968, *Solar Physics* (to be published).
Underwood, J. H., and Muney, W. S. 1967, *Solar Physics*, **1**, 129.
Vaiana, G. S., Reidy, W. P., Zehnpfennig, T., VanSpeybroeck, L., and Giacconi, R. 1968, *Science*, **161**, 564.
White, W. A. 1964*a*, in *AAS-NASA Symposium on the Physics of Solar Flares* (Washington: Scientific and Technical Information Division, NASA), p. 131.
———. 1964*b*, *Space Research IV*, ed. P. Muller (Amsterdam: North-Holland Publishing Co.), pp. 771–779.